L-shell Coster-Kronig transition probabilities in Ni, Cu, and Mo measured with synchrotron radiation

Stacey L. Sorensen,* Stephen J. Schaphorst, Scott B. Whitfield,† and Bernd Crasemann
Department of Physics, University of Oregon, Eugene, Oregon 97403

Roger Carr
Stanford Synchrotron Radiation Laboratory, Stanford, California 94309
(Received 17 December 1990)

A recent technique, based on differential subshell ionization by tuned synchrotron radiation, has been applied to measurements of L-subshell Coster-Kronig yields of Ni, Cu, and Mo from L_2 and L_3 Auger spectra. Results for Ni are $f_{23}=0.6+0.2$, $f_{12}=0.4+0.2$, and $f_{13}=0.5+0.2$; for Cu, $f_{23}=0.8+0.1$, $f_{12}=0.44+0.06$, and $f_{13}=0.3+0.2$; for Mo, $f_{23}=0.15+0.02$, $f_{12}=0.15+0.02$, and $f_{13}=0.61+0.06$. Measured transition probabilities are compared with previously available information. The results are generally consistent with the body of theoretical and experimental data. For Ni and Cu, the present measurements of f_{23} confirm that the L_2-$L_3M_{4,5}$ Coster-Kronig channel is accessible in the metals, even though it is energetically cut off in free atoms. Further improvements in synchrotron-radiation sources are likely to make it possible to throw light on several critical questions by means of the present method.

I. INTRODUCTION

Following ionization in a deep inner shell, atoms deexcite through a cascade of transitions, most of which are radiationless [1–4]. Fastest among these processes are Coster-Kronig transitions [5], through which a vacancy "bubbles up" among the subshells of one shell. The total rate of such Auger transitions among levels with the same principal quantum number is customarily described by a quantity f_{ij}^{X}, defined as the probability that a vacancy in the subshell X_i is shifted by radiationless transitions to the subshell j of the same shell X [1].

In principle, intrashell radiative transitions compete with Coster-Kronig processes [1], but such transitions can ordinarily be neglected. For example, an upper limit of $(1.4\pm3.0)\times10^{-3}$ has been established experimentally for the relative intensity of the radiative component of f_{23}^{L} for Pb, in accord with a theoretical estimate that $2p_{3/2}$-$2p_{1/2}$ electric dipole transitions contribute only $\sim10^{-5}$ of the total L_2 width of Pb [6]. Consequently, interaction between the radiationless and radiative decay channels [7], which in some Auger transitions can result in significant interference effects [8–10], appears to be negligible for Coster-Kronig transitions. Radiationless channel mixing, on the other hand, can substantially affect individual Coster-Kronig rates, redistributing the intensities among component channels without, however, significantly altering the total intensity [11]. Other competing processes are of second order, e.g., the radiative Auger effect or semi-Auger process, in which a photon and an electron are emitted simultaneously [12].

Coster-Kronig transitions are of considerable interest from the point of view of fundamental theory as well as in applications. When they are energetically possible, Coster-Kronig processes are the principal means by which ionized atoms lose energy. In theory, the extraordinary strength of these transitions taxes the limits of perturbative approaches. The rates are exceedingly sensitive to the atomic model as the matrix elements involve the overlap of three bound-state wave functions with a long-wavelength continuum function. Calculated rates vary steeply with transition energy, particularly near threshold [13].

Perhaps most important are the pronounced many-body features that come to play in low-energy Coster-Kronig transitions. Predictions from single-configuration independent-particle calculations disagree strikingly with experimental results. For the much-studied case of Ar, for example, Hartree [14], Hartree-Fock-Slater [15], and Hartree-Fock [16,17] single-configuration calculations overestimate the Ar L_1-$L_{2,3}M_1$ Coster-Kronig rate by a factor of 4 and the ^1P to ^3P intensity ratio for this transition by a factor of 120. Multiconfiguration calculations including the effects of relativity [18] and of exchange and relaxation [17] have reduced these discrepancies. An important correlation effect that influences Coster-Kronig transitions is produced by dynamic relaxation processes or interaction with radiationless continua, in which the core hole fluctuates to intermediate Coster-Kronig levels, in addition to creating electron-hole pair excitations [19–21].

A classic example of these extraordinary manifestations of atomic many-body effects associated with some Coster-Kronig transitions is that of the $[4p]$ hole state in Xe. Here the independent-particle model predicts a radiationless deexcitation rate of astonishing intensity: The hole lifetime is shortened so that ionization and decay processes can no longer be separated clearly. The level becomes so wide that the $4p_{1/2}$ "line" in the photoelectron spectrum virtually disappears [22]. A combination of energy degeneracy and strong overlap between configurations, and of a wide exit channel, produces a situation in which the independent-particle model truly breaks down [23]: Virtual Coster-Kronig transitions cause the

hole to fluctuate with great strength; the level is broadened and redistributed as a result of the many-electron interactions, so that the simple picture of a well-defined hole loses much of its meaning [24]. Rather, the atom behaves more like a breathing plasma, calling for a reformulation of traditional transition theory since the latter is difficult to generalize to the many-electron case involving nonorthogonal orbitals [25]. More recent work on these problems includes the diagrammatic many-body calculations of the Cd *M-NN* Auger spectrum by Ohno and Wendin [26]. Nevertheless, as long as the continuum-electron energy is not too small, it appears that traditional quantum-mechanical approaches often can adequately describe Coster-Kronig processes provided they include (1) configuration interaction and (2) the differences between the potentials in the initial and final states, including effects of relaxation and exchange. Such computations are in progress [27], with indications that they may resolve many of the discrepancies between older theoretical results [28,29] and measurements.

The practical importance of Coster-Kronig transition probabilities is considerable, primarily because they dominate the characteristics of the vacancy cascade that ensues upon inner-shell ionization. The resultant multiple ionization has been estimated by Venugopala Rao *et al.* [30]; a more sophisticated model was constructed by Jacobs *et al.* [31,32]. The results are important for diagnostics of laboratory and astrophysical plasmas and in the design of ion sources; the population inversion can be applied to Auger-pumped short-wavelength lasers [33]. Subshell fluorescence yields depend critically upon Coster-Kronig transition probabilities [1,34]; they are important, for example, in calculations of radiative energy transport through matter, as for radiation-shielding design and in medical radiology, as well as in astrophysics [35]. Interesting suggestions have been made for the use of Coster-Kronig transitions in the diagnostics of the time development of very fast phenomena, such as the ablation of thermonuclear-fusion pellets [36].

Spectra of Coster-Kronig electrons are generally difficult or impossible to measure, because of the very low transition energies. Where such spectra have been obtained, as, e.g., for Ar [37,38], they have been of great value for theoretical analysis [11]. In most cases, the bulk Coster-Kronig transition probabilities f_{ij}^{X} are all that can be determined, and even these have not yet been measured for most elements, or are fraught with large uncertainties [39]. Traditional methods for determining f_{ij}'s have been reviewed in Ref. [1]; they are based primarily on measurements of coincidences between K and L x rays, or between L x rays and nuclear radiation, in the decay of radioactive isotopes. With modern techniques, this approach can lead to good results for the heaviest elements [40–43]. It is not applicable to the L_1 subshell because the K-L_1 radiative transition is dipole forbidden.

A new method for the measurement of Coster-Kronig transition probabilities has become possible with the advent of tunable synchrotron radiation with which subshells can be selectively ionized. This approach was pioneered by Jitschin and collaborators [44–47], who utilized the fact that ionization of a particular subshell can be switched on or off by tuning the incident photon energy across the respective ionization threshold. Detection of the induced fluorescence [46] or Auger-electron emission [47] permits determination of Coster-Kronig transition probabilities and subshell fluorescence yields. Following a report on results obtained for Ag by this technique [48], we describe here an experiment through which the Coster-Kronig transition probabilities f_{ij}^{L} of Ni, Cu, and Mo were measured.

II. EXPERIMENT

A. Method

The method employed in this experiment is based on the tunability of synchrotron radiation, which makes it possible to photoionize the L subshells of sample atoms selectively. Thus, as illustrated in Fig. 1, at some photon energy E_3 only the L_3 subshell is photoionized, with a cross section $\sigma_3(E_3)$, while ionization of the other two L subshells is energetically impossible. At some higher photon energy E_2, both the L_3 and L_2 subshells can be ionized, with cross sections $\sigma_3(E_2)$ and $\sigma_2(E_2)$, respectively. At a still higher photon energy E_1, all three L_i subshells can be photoionized, with respective cross sections $\sigma_i(E_1)$.

Deexcitation of the inner-shell vacancies thus created can be observed by monitoring emitted x rays [46] or Auger electrons [47,48]. For the heavier elements, x-ray detection is of advantage, while for medium-Z and lighter elements with a lower fluorescence yield, the detection of Auger electrons is preferable. Let $N_{A3}(E_3)$ be the observed counting rate in an Auger-electron peak that arises from radiationless transitions to L_3 vacancies created by photoionization with x rays of energy E_3. If now the incident x-ray energy is increased to E_2, ionizing both the L_3 and L_2 subshells, the new Auger counting

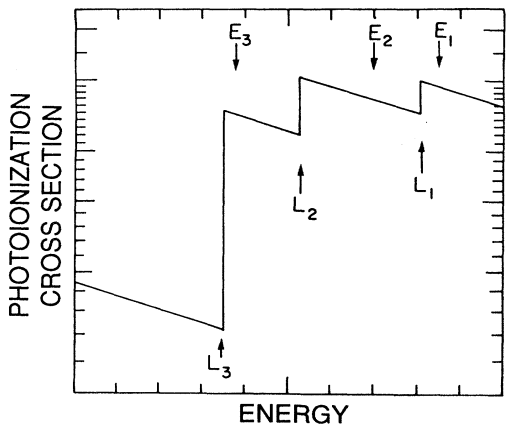

FIG. 1. Schematic representation of L-subshell photoionization cross sections vs x-ray energy, with indication of typical photon energies E_i used in Eqs. (1)–(3).

rate $N_{A3}(E_2)$ will be proportional to the number of L_3 vacancies created by direct L_3 photoioniztion *plus* the number of primary L_2 vacancies that have "bubbled up" to the L_3 subshell with a probability that is the Coster-Kronig yield f_{23}.

It follows that, for constant primary x-ray intensity (photons per second), the Coster-Kronig transition probability f_{23} can be derived from the ratio of the Auger intensities by the relation [48]

$$f_{23}=\left[\frac{N_{A3}(E_2)\sigma_3(E_3)}{N_{A3}(E_3)\sigma_3(E_2)}-1\right]\frac{\sigma_3(E_2)}{\sigma_2(E_2)} . \quad (1)$$

A similar formula describes the number of resultant vacancies transferred from the L_1 subshell to the L_2 subshell following L_1 photoionization:

$$f_{12}=\left[\frac{N_{A2}(E_1)\sigma_2(E_2)}{N_{A2}(E_2)\sigma_2(E_1)}-1\right]\frac{\sigma_2(E_1)}{\sigma_1(E_1)} . \quad (2)$$

Finally, the f_{13} Coster-Kronig yield can be determined from the ratio of the Auger intensity produced through excitation with x rays of energy E_1 to the Auger intensity produced by ionization with x rays of energy E_3:

$$f_{13}=\frac{N_{A3}(E_1)\sigma_3(E_2)}{N_{A3}(E_3)\sigma_2(E_2)}-\frac{\sigma_3(E_1)}{\sigma_1(E_1)} - \left[\frac{\sigma_2(E_1)}{\sigma_1(E_1)}+f_{12}\right]f_{23} . \quad (3)$$

The required subshell photoionization cross sections can be taken from the theoretical work of Scofield [49]. These cross sections were derived from relativistic wave functions and include all relevant multipoles as well as retardation effects. The results are quite accurate (those used here to $\pm\sim 2\%$), as borne out by systematic comparisons with experiment [50] and detailed tests [51].

Suitable Auger spectra are those of the intense L_3-$M_{4,5}M_{4,5}$ and L_2-$M_{4,5}M_{4,5}$ groups [48]. Satellite Auger lines are created when Coster-Kronig transitions take place [52], and their intensity must be taken into account in the analysis of the spectra. The intensity of the exciting radiation needs to be followed; this can be done by measuring the total electron current from a sample mesh placed in the beam, making it possible to account for the effect of changes in the photon flux on the observed Auger intensities.

B. Experimental details

In the present experiment, synchrotron radiation from the SPEAR (Stanford Positron-Electron Accelerator Ring) electron storage ring in the Stanford Synchrotron Radiation Laboratory was used to produce primary vacancies by photoionization of selected inner shells of target atoms. X rays with energy in the 0.8–1.5-keV range were selected from the synchrotron-radiation continuum by Bragg scattering from two beryl [$Be_3Al_2(SiO_2)_6$] crystals in the parallel (1010) configuration in the "JUMBO" monochromator; for (2–4)-keV x rays, two Ge (111) reflections were employed. The full width at half maximum of the monochromatized radiation ranged from 0.6 eV for 1-keV x rays to 0.4 eV for 3-keV x rays. The flux of 3-keV monochromatized photons impinging upon the target was approximately 10^{12} photons per second when the current of 3-GeV electrons in the storage ring was 50 mA [53].

Auger spectra were measured with a Physical Electronics Model No. 15-255 double-pass cylindrical-mirror analyzer. The resolution of the analyzer in the retarding-field mode with the x-ray photoelectron spectroscopy (XPS) aperture at 100-eV pass energy is $\sim 10^{-3}$ [54]. Electrons were detected by a spiraltron electron multiplier operated in the pulse-counting mode; the output pulses were amplified in two stages and shaped for pulse counting. The monchromator, electron spectrometer, and data collection were computer controlled.

Samples were prepared *in situ* by evaporating 2-3 nm of the target metal onto an aluminum substrate. The thickness of the evaporated metal was determined by calibrating the evaporator in a test chamber using a crystal thickness monitor, in which the mass deposited in a fixed area can be deduced from the frequency of vibration of the substrate. The pressure during evaporation was 10^{-9} Torr, and the base pressure of the vacuum chamber was below 10^{-10} Torr during measurements.

The photon flux transmitted by the monochromator was monitored by measuring the electron current emitted by a gold grid (100 lines per inch, 90% transmission) placed in the beam. The number of photons impinging upon the grid was derived from the total current of electrons by means of Au photoabsorption cross sections calculated with the computer code of Berger and Hubbel [55] which provides energy interpolations between the calculated cross sections of Scofield [49]. Grid-current measurements were intercompared with photoelectron-peak intensities measured routinely between Auger-electron scans.

III. RESULTS

A. Data Analysis

The signal-to-noise ratio in all measured Auger spectra was better than 2:1 before background subtraction. Data were corrected for the dependence of the electron-spectrometer transmission on the retarding potential [54]; Cu photoelectron spectra were measured to determine how the spectrometer acceptance changes with analyzer pass energy. The measured Auger spectra were smoothed to remove noise spikes. Line shapes and widths were not altered significantly by this iterative routine. The smoothed spectra were normalized to incident photon flux.

In order to fit the spectra, peak intensities were determined by means of a least-squares minimization routine which includes a background function [56]. The fitting routine relied upon the fact that Auger line shapes are described to first order by a convolution of the natural Lorentzian line profiles of the pertinent atomic levels with the approximately Gaussian transmission function of the spectrometer. The measured Auger peaks were therefore fitted with Pearson-VII functions superimposed

upon the scattered-electron background. The Pearson-VII function [57] can be caused to vary continuously from Lorentzian to Gaussian. It depends upon four parameters: centroid energy, intensity, and two line-shape parameters.

It is well known that measured Auger line shapes can be affected by interactions between the ejected electrons and the sample [58]. Electrons can scatter from atoms bound in the solid lattice, plasmon excitations can appear in the low-energy tails of the peaks, and valence-electron excitations can cause strong low-energy dispersion of the electrons. Auger-electron emission can also be accompanied by excitation of other atomic electrons to higher bound or continuum states. Distortions of the electron spectra were modeled by a routine developed by Weightman *et al.* [56]. The Weightman line-shape function takes into account the asymmetries due to plasmons, valence-electron excitations, and phonon energy loss. This function includes a level subtraction which is determined from the number of counts on the extreme high-energy side of the spectrum, and a step function which is derived from the fitted peak parameters. The background function [56] is

$$y(E)=a_1(E)+\frac{a_2(E)a_3a_4}{1+\exp(x-x_0/0.34a_0)} . \quad (4)$$

Here, a_2 and a_0 are parameters of the Pearson-VII line-shape function. The three parameters a_1, a_3, and a_4 were determined by fitting L photoelectron peaks. Fitted $L_{2,3}$-$M_{4,5}M_{4,5}$ Auger spectra of Ni, Cu, and Mo are shown in Figs. 2 and 3.

B. Shake satellites

Photoionization of atomic core electrons is often accompanied by excitation of a second electron, producing

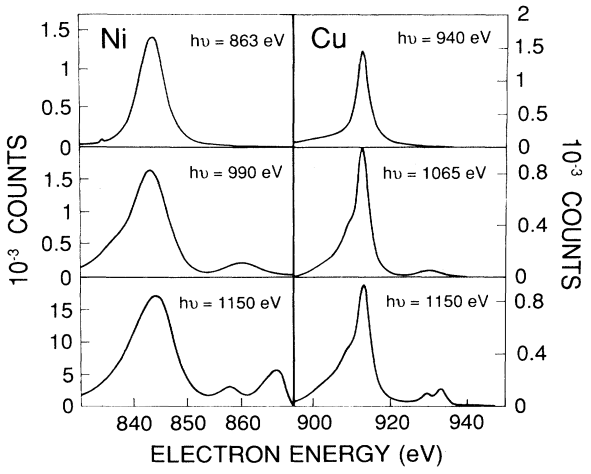

FIG. 2. Fitted Ni (left) and Cu (right) $L_{2,3}$-$M_{4,5}M_{4,5}$ Auger spectra excited with x rays of the energies indicated in each panel. The spectra have been normalized to incident x-ray flux and corrected for changes in photoionization cross section with x-ray energy, as described in the text.

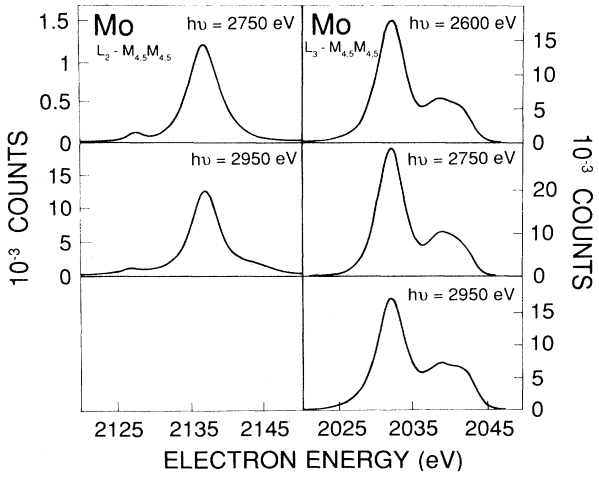

FIG. 3. Fitted Mo L_2-$M_{4,5}M_{4,5}$ (left) and L_3-$M_{4,5}M_{4,5}$ (right) Auger spectra excited with x rays of the energies indicated in each panel. Normalization to x-ray flux and correction for energy dependence of photoionization cross sections were performed as in Fig. 2.

a "spectator" vacancy and causing the energy of subsequently emitted Auger electrons to be shifted into satellite peaks. For the present purposes, the intensity of these satellites must be included in the total Auger intensity. Multiple excitation processes during photoionization are a direct consequence of many-electron correlations between atomic electrons [59]. The atomic electrons experience a perturbation when the effective potential of the atom changes during inner-shell ionization. At large photon energies, the sudden approximation of perturbation theory is valid since the effective charge seen by the atomic electrons changes very quickly [52]. In the conventional sudden approximation [59], the wave functions of the atomic core are assumed to be "frozen:" The removed electron is taken to leave the atom before the remaining atomic-electron orbitals have time to relax. Based on this *ansatz,* independent-particle shakeoff probabilities for the present experiment were calculated with frozen-orbital Hartree-Fock wave functions from the code of Froese-Fischer [60]. Results are listed in Table I.

TABLE I. Calculated shakeoff probabilities (in percent).

	Photoionized electron					
Shake	Nickel		Copper		Molybdenum	
orbital	2*s*	2*p*	2*s*	2*p*	2*s*	2*p*
3*s*	0.2	0.2	0.2	0.2		
3*p*	1.3	1.4	1.1	1.2	0.5	0.6
3*d*	12.3	12.2	12.0	12.0	1.8	1.9
4*s*	12.9	13.3	12.5	13.0	0.6	0.7
4*p*					3.0	3.1
4*d*					18.3	18.2
5*s*					8.2	8.3

TABLE II. Calculated Ni, Cu, and Mo L_3–$M_{4,5}M_{4,5}$ $^1G_4$ diagram-line and satellite Auger energies.

Element	Spectator vacancies	Auger energy (eV)
$_{28}$Ni		841.6
	$3d$	837.6
	$3d^2$	831.7
$_{29}$Cu		918.8
	$3s$	916.0
	$3p$	914.4
	$3d$	914.7
	$3d^2$	912.1
$_{42}$Mo		2031.86
	$4d$	2017.46
	$4p$	2014.86
	$4s$	2013.86
	$3d$	1996.17
	$3d^2$	1966.16

TABLE III. Measured relative intensities of Ni, Cu, and Mo *L-MM* Auger groups excited at various photon energies, normalized to incident photon flux.

Element	Transition	Photon energy (eV)	Relative intensity
$_{28}$Ni	L_3-$M_{4,5}M_{4,5}$	865	1.13±0.07
		990	1.22±0.05
		1150	0.99±0.07
	L_2-$M_{4,5}M_{4,5}$	990	16.6±0.9
		1150	16.4±0.8
$_{29}$Cu	L_3-$M_{4,5}M_{4,5}$	940	2.19±0.05
		1065	2.36±0.04
		1150	2.01±0.03
	L_2-$M_{4,5}M_{4,5}$	1065	2.42±0.04
		1150	2.31±0.04
$_{42}$Mo	L_3-$M_{4,5}M_{4,5}$	2600	6.76±0.05
		2750	6.33±0.04
		2950	5.74±0.04
	L_2-$M_{4,5}M_{4,5}$	2750	3.9±0.2
		2950	3.2±0.2

The energies of the Auger satellite lines emitted in the presence of these spectator vacancies were calculated in order to account for any loss in measured diagram-line Auger intensity due to shake processes [61]. These calculations were performed by the "ΔSCF" (self-consistent-field difference) approach; corrections for extra-atomic relaxation and chemical shifts were applied according to the method of Ohno and Wendin [62] as described in detail in Ref. [48]. Results are listed in Table II.

C. Experimental results

Results of the analysis of Ni, Cu, and Mo Auger spectra excited at various x-ray energies are collected in Table III. The *L*-shell Coster-Kronig yields derived from the relative Auger intensities through Eqs. (1)–(3) are shown in Table IV, which for the sake of completeness also includes results for Ag reported previously in Ref. [48]. Theoretical [15,29,63] and semiempirical [39] Coster-Kronig yields are also shown in Table IV for purposes of comparison.

IV. DISCUSSION

Results of the present measurements, including those reported in Ref. [48], are plotted in Fig. 4. The probable errors are relatively large because the subtractions of terms in Eqs. (1)–(3) tend to emphasize the errors that originate from fitting of the spectra—particularly if the ratio of photoionization cross sections is large. In further experiments with new synchrotron-radiation sources that provide higher flux, it will probably be possible to attain much greater precision. Despite their relative crudity, the present measurements contain some interesting information.

In Fig. 4 we have included curves which represent the semiempirical Coster-Kronig yields of Krause [39]; these represent a set of mutually consistent values compatible with experimental and theoretical information available in the late 1970's. These curves are a useful guide to systematic trends of atomic inner-shell radiative and radiationless yields.

TABLE IV. *L*-shell Coster-Kronig yields f_{ij} of Ni, Cu, Mo, and Ag.

	f_{12}			f_{13}			f_{23}		
Element	Experiment[a]	Theory	Semiemp.[b]	Experiment[a]	Theory	Semiemp.[b]	Experiment[a]	Theory	Semiemp.[b]
$_{28}$Ni	0.35±0.20	0.28[c]	0.30	0.5±0.2	0.23[c]	0.55	0.6±0.2	0.03[d]	0.028
		0.325[e]			0.622[e]				
$_{29}$Cu	0.44±0.06	0.28[c]	0.30	0.3±0.2	0.23[c]	0.54	0.8±0.1	0.03[d]	0.028
		0.32[e]			0.62[e]				
$_{42}$Mo	0.15±0.02	0.07[c]	0.10	0.61±0.06	0.76[c]	0.61	0.15±0.02	0.14[c]	0.144
		0.05[f]			0.69[f]			0.124[e]	
		0.166[e]			0.689[e]				
$_{47}$Ag	0.044±0.004	0.068[g]	0.10	0.61±0.06	0.74[g]	0.59	0.17±0.03	0.155[g]	0.153
		0.064[f]			0.70[f]			0.152[e]	
		0.052[e]			0.786[e]				

[a]Present work.
[b]Reference [39].
[c]Reference [29], interpolated.
[d]Calculated for *free* atoms; see text.
[e]Reference [15].
[f]Reference [63].
[g]Reference [29].

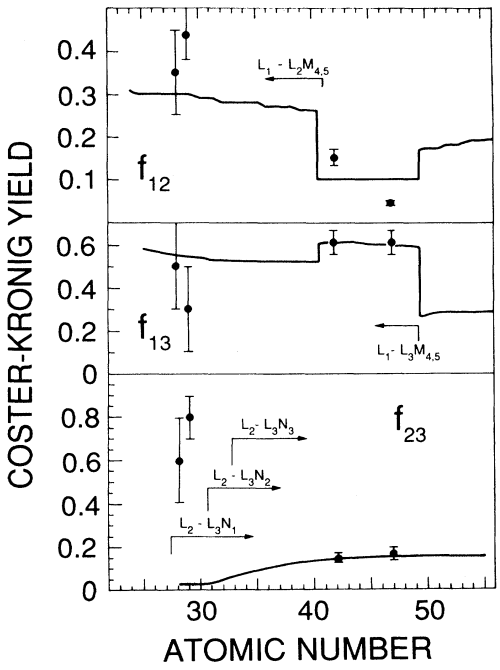

FIG. 4. Coster-Kronig yields measured in the present work (points with error bars) compared with the semiempirical fit of Krause (Ref. [39]) (solid curves), as functions of atomic number. Thresholds for some dominant transitions are indicated.

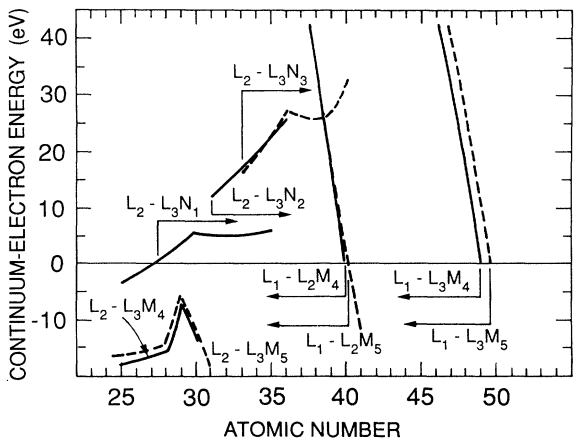

FIG. 5. Near-threshold Coster-Kronig-electron energies for some dominant transitions, calculated for *free* atoms (Ref. [64]), as functions of atomic number. Thresholds of relevant transitions are indicated by vertical lines, with horizontal arrows pointing into regions where these transitions can take place.

A striking feature of the L_1-shell Coster-Kronig yields is the sudden drop in f_{12} between $_{40}$Zr and $_{41}$Nb, caused by the energy cutoff of L_1-$L_2M_{4,5}$ transitions, and a similar drop in f_{13} from $_{49}$In to $_{50}$Sn, due to the cutoff of L_1-$L_3M_{4,5}$ transitions. Concomitant rises take place in f_{13} and f_{12}, respectively, between these atomic numbers, because the f_{ij} are not independent; by virtue of their definitions [1], the L-subshell fluorescence yields ω_i, Auger yields a_i, and Coster-Kronig yields f_{ij} are interconnected by the relation

$$\omega_i + a_i + \sum_{\substack{i,j \\ j=i+1}}^{3} f_{ij} = 1 \ . \tag{5}$$

The energy cutoffs which cause the abrupt drops in f_{12} and f_{13} that appear in the curves in Fig. 4 are in accord with relativistic ΔSCF calculations for free atoms [64], as plotted in Fig. 5. Once a Coster-Kronig transition becomes energetically allowed (continuum-electron energy greater than 0 in Fig. 5), its rate usually rises quickly with increasing transition energy because there are no close-in nodes in the low-energy continuum wave function of the Auger electron, and hence, no cancellations in the matrix element [65].

The rapid rise of Coster-Kronig transition rates beyond thresholds also explains the increase in f_{23} between atomic numbers 30 and 40, where the N shell is being filled, allowing the onset of intense L_2-$L_3N_{1,2,3}$ transitions.

The relatively precise measurement [48] of f_{12} for Ag indicates a yield that is only one-half of that given by the Krause curve [39] in this neighborhood of the periodic table. This result may point toward a systematic deviation from the curve; calculated values of f_{12} for Ag (Refs. [15], [29], and [63]) and Rh (Ref. [29]) also point in this direction.

An interesting situation arises in connection with the Coster-Kronig yields f_{23} of Ni and Cu. According to free-atom energy calculations [64], L_2-L_3N_1 is the only possible transition that can contribute to f_{23} for these elements (Fig. 5); its rate according to a relativistic Dirac-Hartree-Slater calculation [28] is 0.70 milliatomic units near $Z=30$, which corresponds to a partial width of ~0.02 eV. The total L_2 level width of Cu has been measured [65] to be 0.98±0.04 eV; a semiempirical linewidth fit [66] leads to a Cu L_2 width of 0.70 eV. It follows that, if L_2-L_3N_1 were indeed the only channel, the ratio f_{23} of partial to total width would be in the range from 0.02 to 0.03, which is in accord with Krause's table [39]. On the other hand, there has been strong evidence that L_2-$L_3M_{4,5}$ transitions, cut off in free Cu atoms (Fig. 5), are in fact possible in *metallic* copper, thanks primarily to extra-atomic relaxation effects [67]; an early indication that these transitions are possible in Cu metal was seen in the fact that the measured L_2 width of Zn is *smaller* than that of Cu, contrary to the general trend [65]. Satellites in the L_3-$M_{4,5}M_{4,5}$ Auger spectra of Cu and Zn have traditionally been ascribed to an $M_{4,5}$ spectator vacancy created by preceding L_2-$L_3M_{4,5}$ Coster-Kronig transitions [67]. This fact has recently been confirmed by a synchrotron-radiation-excited soft-x-ray-fluorescence study of Cu and Zn [68]. If the intense L_2-$L_3M_{4,5}$ transitions are allowed in Cu, then f_{23} should be in the neighborhood of 0.64, according to a calculation based on Green's atomic independent-particle potential [65]. The present measurements appear to bear out this prediction.

It can be anticipated that the new third-generation synchrotron-radiation facilities that are currently being constructed or planned will make it possible to apply the differential subshell excitation method to far more precise studies of Coster-Kronig yields than has been possible in the present work, shedding light on some of the fascinating questions that remain unanswered in this field [69].

ACKNOWLEDGMENTS

We thank Wolfgang Jitschin for help and advice in the initial stages of the experiment, and George S. Brown and Teijo Åberg for helpful discussions. Matt Richter, Mike Rowan, Ann Waldhauer, and Joe Woicik rendered indispensable technical assistance. This research was supported in part by the National Science Foundation through Grants Nos. PHY-8516788, PHY-8908124, and PHY-9014517. The experiment was performed in the Stanford Synchrotron Radiation Laboratory which is supported by the U.S. Department of Energy through the office of Basic Energy Sciences and by the National Institutes of Health through the Biotechnology Resources Program.

*Present address: Department of Physics I, Royal Institute of Technology, S-10044 Stockholm, Sweden.

†Present address: Department of Physics, University of Central Florida, Orlando, FL 32816.

[1] W. Bambynek, B. Crasemann, R. W. Fink, H.-U. Freund, H. Mark, C. D. Swift, R. E. Price, and P. Venugopala Rao, Rev. Mod. Phys. **44**, 716 (1972).

[2] E. H. S. Burhop and W. N. Asaad, Adv. At. Mol. Phys. **8**, 163 (1972).

[3] M. H. Chen, in *Atomic Inner-Shell Physics,* edited by B. Crasemann (Plenum, New York, 1985), Chap. 2.

[4] W. Mehlhorn, in *Atomic Inner-Shell Physics* (Ref. [3]), Chap. 4.

[5] D. Coster and R. de L. Kronig, Physica **2**, 13 (1935).

[6] M. H. Chen, B. Crasemann, P. Venugopala Rao, J. M. Palms, and R. E. Wood, Phys. Rev. A **4**, 846 (1971).

[7] T. Åberg, in *Inner-Shell and X-Ray Physics of Atoms and Solids,* edited by D. J. Fabian, H. Kleinpoppen, and L. M. Watson (Plenum, New York, 1981), p. 251.

[8] L. Armstrong, Jr., C. E. Theodosiou, and M. J. Wall, Phys. Rev. A **18**, 2538 (1978).

[9] V. L. Jacobs, Phys. Rev. A **31**, 383 (1985).

[10] T. Åberg and G. Howat, *Theory of the Auger Effect,* edited by W. Mehlhorn, Handbuch der Physik Vol. 31 (Springer-Verlag, Berlin, 1982), p. 469.

[11] K. R. Karim and B. Crasemann, Phys. Rev. A **31**, 709 (1985).

[12] T. Åberg, in *Atomic Inner-Shell Processes,* edited by B. Crasemann (Academic, New York, 1975), Vol. I, Chap. 9.

[13] M. H. Chen, B. Crasemann, L. I Yin, T. Tsang, and I. Adler, Phys. Rev. A **13**, 1435 (1976).

[14] A. Rubenstein, Ph.D. thesis, University of Illinois, Urbana, 1955.

[15] E. J. McGuire, in *Atomic Inner-Shell Processes* (Ref. [12]), Vol. I, p. 293; Phys. Rev. A **3**, 587 (1971); **3**, 1801 (1971).

[16] K. G. Dyall and F. P. Larkins, J. Phys. B **5**, 4103 (1982).

[17] K. R. Karim, M. H. Chen, and B. Crasemann, Phys. Rev. A **29**, 2605 (1984).

[18] J. Bruneau, J. Phys. B **16**, 4135 (1983).

[19] D. R. Beck and C. A. Nicolaides, in *Excited States in Quantum Chemistry,* edited by C. A. Nicolaides and D. R. Beck (Reidel, Dordrecht, 1978).

[20] M. Ohno and G. Wendin, J. Phys. B **11**, 1557 (1979); **12**, 1305 (1979); G. Wendin, in *X-Ray and Atomic Inner-Shell Physics 1982,* edited by B. Crasemann, AIP Conference Proceedings No. 94 (AIP, New York, 1982), p. 495.

[21] M. H. Chen, B. Crasemann, and H. Mark, Phys. Rev. A **24**, 1158 (1981).

[22] U. Gelius, J. Electron Spectrosc. Relat. Phenom. **5**, 985 (1974).

[23] M. O. Krause, in *Photoionization and Other Probes of Many-Electron Interactions,* edited by F. Wuilleumier (Plenum, New York, 1976).

[24] G. Wendin and M. Ohno, in *Proceedings of the Second International Conference on Inner-Shell Ionization Phenomena, Freiburg, 1976, Invited Papers,* edited by R. Brenn and W. Mehlhorn (Fakultät für Physik, Universität Freiburg, 1976), p. 166.

[25] G. Howat, T. Åberg, and O. Goscinski, J. Phys. B **11**, 1575 (1978); T. Åberg, in *Inner-Shell and X-Ray Physics of Atoms and Solids,* edited by D. J. Fabian, H. Kleinpoppen, and L. M. Watson (Plenum, New York, 1980), p. 251.

[26] M. Ohno and G. Wendin, J. Phys. C **14**, L1133 (1981).

[27] A. Mäntykenttä, B. Crasemann, S. L. Sorensen, and M. H. Chen, in Book of Abstracts, Fifteenth International Conference on X-Ray and Inner-Shell Processes, Knoxville, Tennessee, 1990, edited by M. O. Krause (unpublished), p. G03.

[28] M. H. Chen, B. Crasemann, and H. Mark, At. Data Nucl. Data Tables **24**, 13 (1979).

[29] M. H. Chen, B. Crasemann, and H. Mark, Phys. Rev. A **24**, 177 (1981).

[30] P. Venugopala Rao, M. H. Chen, and B. Crasemann, Phys. Rev. A **5**, 997 (1972).

[31] V. L. Jacobs, J. Davis, B. F. Rozsnyai, and J. W. Cooper, Phys. Rev. A **21**, 1917 (1980).

[32] V. L. Jacobs and B. F. Rozsnyai, Phys. Rev. A **34**, 216 (1986).

[33] H. C. Kapteyn and R. W. Falcone, Phys. Rev. A **37**, 2033 (1988); see also E. J. McGuire and M. A. Duguay, Appl. Opt. **16**, 83 (1977); C. P. J. Barty, D. A. King, G. Y. Yin, K. H. Hahn, J. E. Field, J. F. Young, and S. E. Harris, Phys. Rev. Lett. **61**, 2201 (1988).

[34] J. Auerhammer, H. Genz, and A. Richter, Z. Phys. D **7**, 301 (1988).

[35] T. E. Bunch, L. J. Caroff, and H. Mark, in *Atomic Inner-Shell Processes* (Ref. [12]), Vol. II, p. 187.

[36] S. V. Bobashev (private communication).

[37] W. Mehlhorn, Z. Phys. **208**, 1 (1968).

[38] J. Nordgren, H. Ågren, L. Selander, C. Nordling, and K. Siegbahn, Phys. Scr. **16**, 70 (1977); **19**, 5 (1979).

[39] M. O. Krause, J. Phys. Chem. Ref. Data **8**, 307 (1979).

[40] J. L. Campbell, P. L. McGhee, R. R. Gingerich, R. W. Ollerhead, and J. A. Maxwell, Phys. Rev. A **30**, 161 (1984).
[41] J. L. Campbell, P. L. McGhee, J. A. Maxwell, R. W. Ollerhead, and B. Wittaker, Phys. Rev. A **33**, 986 (1986).
[42] J. L. Campbell and P. L. McGhee, J. Phys. (Paris) Colloq. **48**, C9-597 (1987).
[43] A. L. Catz, Phys. Rev. A **36**, 3155 (1987); **40**, 4977 (1989).
[44] W. Jitschin, G. Materlik, U. Werner, and P. Funke, J. Phys. B **18**, 1139 (1985).
[45] W. Jitschin, U. Werner, K. Finck, and H. O. Lutz, in *High-Energy Ion-Atom Collisions II,* edited by D. Berényi and G. Hock (North-Holland, Amsterdam, 1985), p. 79.
[46] U. Werner and W. Jitschin, Phys. Rev. A **38**, 4009 (1988).
[47] W. Jitschin, G. Grosse, and P. Rohl, Phys. Rev. A **39**, 103 (1989).
[48] S. L. Sorensen, R. Carr, S. J. Schaphorst, S. B. Whitfield, and B. Crasemann, Phys. Rev. A **39**, 6241 (1989).
[49] J. H. Scofield, Lawrence Livermore Radiation Laboratory Report No. UCRL-51326, 1973 (unpublished).
[50] J. H. Hubbell and W. J. Veigele, *Comparison of Theoretical and Experimental Photoeffect Data 0.1 keV to 1.5 MeV,* Natl. Bur. Stand. (U.S.) Technical Report No. 901 (U.S. GPO, Washington, DC, 1976).
[51] W. Jitschin, U. Werner, G. Materlik, and G. D. Doolen, Phys. Rev. A **35**, 5038 (1987).
[52] G. B. Armen, Ph.D thesis, University of Oregon, 1985; B.Crasemann, J. Phys. (Paris) Colloq. **48**, C9-389 (1987).
[53] F. D. Dikmen (unpublished); Z. Hussain, E. Umbach, D. A. Shirley, J. Stöhr, and J. Feldhaus, Nucl. Instrum. Methods **195**, 115 (1982).
[54] P. W. Palmberg, J. Electron Spectrosc. Relat. Phenom. **5**, 691 (1974).
[55] M. J. Berger and J. H. Hubbel, XCOM: Photon Cross Sections on a Personal Computer, Natl. Bur. Stand. (U.S.) Report No. NBSIR 87-3597, 1978 (unpublished).
[56] P. Weightman, E. D. Roberts, and C. E. Johnson, J. Phys. C **8**, 550 (1975).
[57] K. Pearson, Biometrika **16**, 157 (1924).
[58] K. Sevier, *Low-Energy Electron Spectrometry* (Wiley-Interscience, New York, 1972).
[59] T. Åberg, Ann. Acad. Sci. Fenn. Ser. A6 **308**, 1 (1969).
[60] C. Froese-Fischer, Comput. Phys. Commun. **14**, 145 (1978).
[61] D. Burch, L. Wilets, and W. E. Meyerhof, Phys. Rev. A **9**, 1007 (1974).
[62] M. Ohno and G. Wendin, J. Phys. C **15**, 1787 (1982).
[63] B. Crasemann, M. H. Chen, and V. O. Kostroun, Phys. Rev. A **4**, 2161 (1971).
[64] M. H. Chen, B. Crasemann, K.-N. Huang, M. Aoyagi, and H. Mark, At. Data Nucl. Data Tables **19**, 97 (1977).
[65] L. I Yin, I. Adler, M. H. Chen, and B. Crasemann, Phys. Rev. A **7**, 897 (1973).
[66] M. O. Krause and J. H. Oliver, J. Phys. Chem. Ref. Data **8**, 329 (1979).
[67] N. Mårtensson and B. Johansson, Phys. Rev. B **28**, 3733 (1983), and references therein.
[68] N. Wassdahl, J.-E. Rubensson, G. Bray, P. Glans, P. Bleckert, R. Nyholm, S. Cramm, N. Mårtensson, and J. Nordgren, Phys. Rev. Lett. **64**, 2807 (1990).
[69] W. Jitschin, in *Proceedings of the Fifteenth International Conference on X-Ray and Inner-Shell Processes,* edited by M. O. Krause (American Institute of Physics, New York, 1990), p. 408.